Energy-efficient Signalling in QoS Constrained Heterogeneous Networks

Nguyen, L. D., Tuan, H. D., & Duong, T. Q. (2016). Energy-efficient Signalling in QoS Constrained Heterogeneous Networks. IEEE Access. DOI: 10.1109/ACCESS.2016.2626363

Published in:
IEEE Access

Document Version:
Publisher's PDF, also known as Version of record

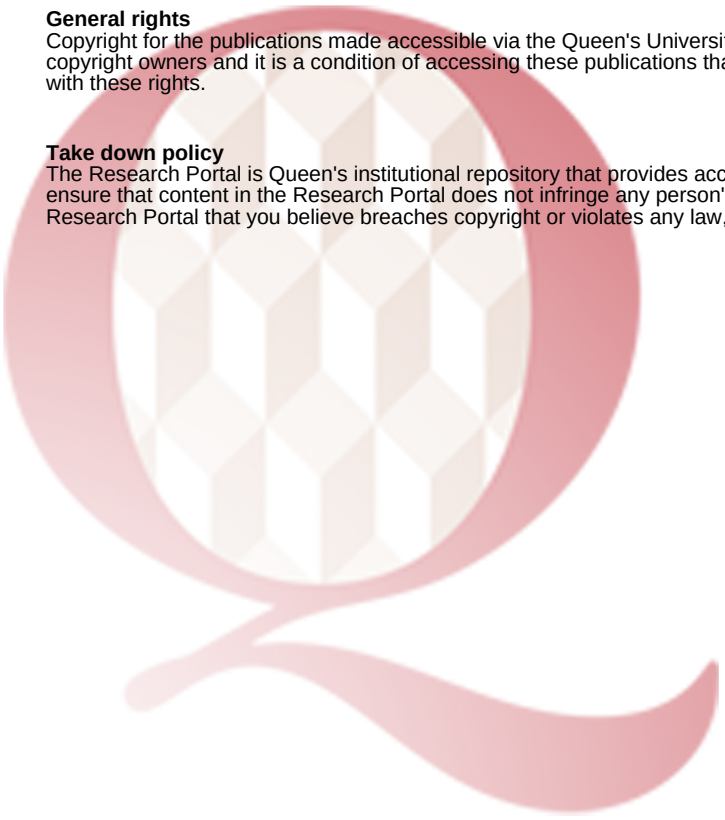

This article has been accepted for publication in a future issue of this journal, but has not been fully edited. Content may change prior to final publication. Citation information: DOI 10.1109/ACCESS.2016.2626363, IEEE Access

Energy-efficient Signalling in QoS Constrained Heterogeneous Networks

Long D. Nguyen, Hoang D. Tuan and Trung Q. Duong

***Abstract*—This paper considers a heterogeneous network (HetNet), which consists of one macro base station (MBS) and numerous small cell base stations (SBSs) cooperatively serving multiple user terminals. The first objective is to design cooperative transmit beamformers at the base stations to maximize the network energy efficiency (EE) in terms of bits per Joule subject to the users' quality of service (QoS) constraints, which poses a computationally difficult optimization problem. The commonly used Dinkelbach-type algorithms for optimizing a ratio of concave and convex functions are not applicable. The paper develops a path-following algorithm to address the computational solution to this problem, which invokes only a simple convex quadratic program of moderate dimension at each iteration and quickly converges at least to a locally optimal solution. Furthermore, the problem of joint beamformer design and SBS service assignment in the three-objective (EE, QoS and service loading) optimization is also addressed. Numerical results demonstrate the performance advantage of the proposed solutions.**

***Index Terms*—Heterogeneous networks, energy efficiency, QoS constraint, service loading, fractional programming, path-following method.**

I. Introduction

Heterogeneous networks (HetNets) have recently been considered as a solution for supporting the unprecedented data increase and consistent quality of service (QoS) within the fifth-generation wireless networks (5G) [1]–[3]. A HetNet consists of macro base stations (MBSs) and small-cell base stations (SBSs) with low power consumption and short range of coverage, which are densely deployed in different locations to bring them closer to the users so as to improve QoS and reduce the radiated signal power. A key challenge for the successful deployment of such HetNets is to efficiently handle the intra- and inter-tier interference [4], [5].

L. D. Nguyen, and T. Q. Duong are with Queen's University Belfast, U.K. (email: {lnguyen04, trung.q.duong}@qub.ac.uk).

H. D. Tuan is with University of Technology Sydney, Sydney, Australia (email: Tuan.Hoang@uts.edu.au).

This work was supported in part by the U.K. Royal Academy of Engineering Research Fellowship under Grant RF1415\14\22 and by the Newton Institutional Link under Grant ID 172719890.

On the other hand, the larger amount of hardware and infrastructure needed for numerous base stations in HetNets leads to a substantial increase of the circuit power consumption, which is a serious ecological and economical concern [6]. In fact, the energy efficiency (EE) in terms of bits per Joule is another figure of merit in assessing 5G systems [7], [8]. An actice/sleep (on/off) regime for MBSs to save the HetNet energy was proposed in [9], while configuration guidelines for energy-efficient HetNets consisting of massive multiple-input multiple-output (MIMO) MBSs and SBSs were provided in [10]–[12].

It should be noted that the design of transmit beamformer for the network EE is different from that for conventional beamformer power optimization, which aims at minimizing the beamforming power subject to the users' QoS throughput (see e.g. [13], [14] and references therein). The objective in EE is a ratio of the network sum throughput and the total power consumption, which includes the beamformer power, so maximizing the EE objective does not quite mean minimizing the beamformer power. In our previous work [15], we have optimized the network EE performance using the Dinkelbach's method and a novel group sparsity for joint linear precoder design and small-cell switching-off approach. However, the existing approaches to EE maximization use the Dinkelbach-type algorithms [16] of fractional programming as the main tool for obtaining computational solutions (see e.g. [17]–[19] and references therein). Realizing the shortage of [17], [18] in guaranteeing the QoS in terms of the users' throughput thresholds in maximizing EE, which causes undesirable QoS discrimination, the authors of [19] considered EE in a QoS constrained context. Each Dinkelbach's iteration then constitutes a difficult nonconvex program, which was addressed in [19] by semi-definite relaxation (SDR). As analysed in details in [20], SDR not only increases the problem dimension substantially but performs very poorly whenever its rank-one matrix solution cannot be found. Moreover, SDR in [19] involves a logarithm function optimization, which is convex but quite computationally consuming.

In this paper, we consider a two-tier cooperative

This article has been accepted for publication in a future issue of this journal, but has not been fully edited. Content may change prior to final publication. Citation information: DOI 10.1109/ACCESS.2016.2626363, IEEE Access

network, which consists of a MBS and numerous SBSs cooperating in serving multiple user terminals with QoS. The research contributions are detailed as follows.

- A novel path-following computational procedure is proposed, which invokes a simple convex quadratic program of moderate size at each iteration and converges to at least a locally optimal solution.
- An effective computational solution for another important problem in the three-objective (EE, QoS and BS service loading) optimization is also proposed. In this solution, service loading refers to the number of users that a BS should serve.

The paper is structured as follows. After the Introduction, Section II introduces the EE maximization problems and also analyses its computational challenges. Its path-following computational procedure is developed in Section III. Section IV considers a solution for the three-objective optimization problems.

Notation. Boldface upper and lowercase letters denote matrices and (column or row) vectors, respectively. The transposition and conjugate transposition of matrix $\boldsymbol{X}$ are respectively represented by $\boldsymbol{X}^T$ and $\boldsymbol{X}^H$. $\boldsymbol{I}$ and $\boldsymbol{0}$ stand for identity and zero matrices of appropriate dimensions. $\Re\{\cdot\}$ denotes the real part of its argument. $||\boldsymbol{x}||$ and $||\boldsymbol{X}||$ are Euclidean norm of vector $\boldsymbol{x}$ and Frobenius norm of matrix $\boldsymbol{X}$, respectively. $\mathcal{CN}(0,\sigma_x^2)$ is referred to Gaussian white noise with power σ_x^2 . For matrices $\boldsymbol{X}_1,...,\boldsymbol{X}_k$ of same column number, the matrix $[\boldsymbol{X}_1;...;\boldsymbol{X}_k]$ is created by vertically stacking $\boldsymbol{X}_1,...,\boldsymbol{X}_k$.

II. Problem statement

We consider a downlink two-tier network, in which one MBS referred to as BS 0 and S small cell base stations (SBSs) referred to as SBS 1, ..., SBS S share the same frequency spectrum as illustrated by Fig. 1. The set of BSs is $\mathcal{S} = \{0, 1, ..., S\}$. The MBS is equipped with M_0 antennas while each SBS s is equipped with M antennas. In what follows, define $M_s = M_0$ for $s = 0$ and $M_s = M$ for $s \neq 0$. The total transmit antenna number is $M_t = M_0 + SM$. All BSs, which are connected to a central processor (CP) via backhaul links, are supposed to cooperate to serve K users, each of which is equipped by a single antenna.

It is assumed that the CP has access to global channel state information $\boldsymbol{h}_k^s \in \mathbb{C}^{1\times M_s}$ between BS s and user k. All BSs cooperate to convey symbol x_k with the normalized power $\mathcal{E}(x_k^2) = 1$ to user $k \in \mathcal{K} = \{1, \cdots, K\}$, which is beamformed by $\mathbf{f}_k^s \in \mathbb{C}^{M_s}$ at BS s before

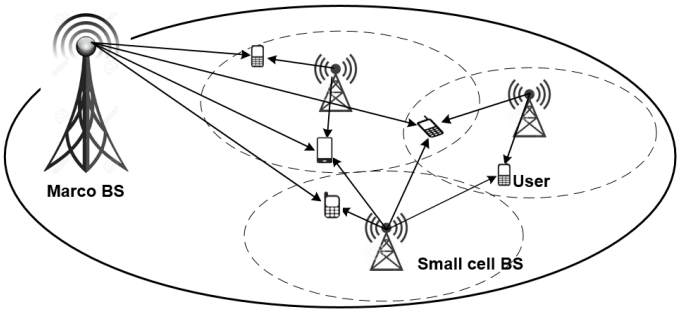

Fig. 1. An example model for the downlink HetNets.

transmission. The received signal at user k is given by

$$y_k = \left(\sum_{s=0}^{S} \boldsymbol{h}_k^s \boldsymbol{f}_k^s\right) x_k + \sum_{i\in\mathcal{K}\setminus\{k\}} \left(\sum_{s=0}^{S} \boldsymbol{h}_k^s \boldsymbol{f}_i^s\right) x_i + n_k, \tag{1}$$

where n_k is the additive white Gaussian noise $\mathcal{CN}(0,\sigma_k^2)$. The first summation term in (1) represents the desired signal, while the second and third terms express the multiple user interference and noise, respectively.

To suppress the interference in (1), we employ the block diagonalization [21] to make zero-forcing

$$\sum_{s=0}^{S} \boldsymbol{h}_k^s \boldsymbol{f}_i^s = 0 \ \forall i \neq k. \tag{2}$$

For

$$\boldsymbol{h}_k \triangleq \left[\boldsymbol{h}_k^0, \boldsymbol{h}_k^1, ..., \boldsymbol{h}_k^S\right] \in \mathbb{C}^{1\times M_t}$$

and

$$\boldsymbol{f}_k \triangleq \left[\boldsymbol{f}_k^0;\ \boldsymbol{f}_k^1;\ ...;\ \boldsymbol{f}_k^S\right] \in \mathbb{C}^{M_t}, \tag{3}$$

equation (1) is rewritten by

$$y_k = \boldsymbol{h}_k \boldsymbol{f}_k x_k + \sum_{i\in\mathcal{K}\setminus\{k\}} \boldsymbol{h}_k \boldsymbol{f}_i x_i + n_k. \tag{4}$$

Under the zero-forcing condition (2), the information throughput (in nats) at user k is

$$C_k(\boldsymbol{f}_k) = \ln(1 + |\boldsymbol{h}_k \boldsymbol{f}_k|^2/\sigma_k^2). \tag{5}$$

On the other hand, for $\mathbf{F} \triangleq (\mathbf{f}_1, \ldots, \mathbf{f}_K)$, the total power consumption for the downlink transmission is calculated by [10], [22]

$$P^{\mathsf{total}}(\mathbf{F}) = \sum_{s=0}^{S} \frac{1}{\lambda_s} \sum_{k=1}^{K} ||\mathbf{f}_k^s||^2 + P^{\mathsf{cir}}, \tag{6}$$

where $\lambda_s \in (0, 1)$ is the power efficiency of the amplifier of BS s and $P^{\mathsf{cir}} = M_0 P_m + \sum_{s=1}^{S} M_s P_n + \sum_{s=0}^{S} P_{c,s}$ is the total circuit power to operate BSs. Therein, P_m and

This article has been accepted for publication in a future issue of this journal, but has not been fully edited. Content may change prior to final publication. Citation information: DOI 10.1109/ACCESS.2016.2626363, IEEE Access

P_n represent the per-antenna circuit power of MBS and SBSs, respectively. $P_{c,s}$ is defined as non-transmission power of BSs.

Define

$$\widetilde{\boldsymbol{H}}_k^s \triangleq \left[\boldsymbol{h}_1^s; ...; \boldsymbol{h}_{k-1}^s; \boldsymbol{h}_{k+1}^s; ...; \boldsymbol{h}_K^s\right] \in \mathbb{C}^{(K-1)\times M_s},$$

which is created by vertically stacking all the vector channels from BS s to all users but user k, and

$$\widetilde{\boldsymbol{H}}_k \triangleq \left[\widetilde{\boldsymbol{H}}_k^0, \widetilde{\boldsymbol{H}}_k^1, ..., \widetilde{\boldsymbol{H}}_k^S\right] \in \mathbb{C}^{(K-1)\times M_t}.$$

The zero-forcing condition (2) then means that $\boldsymbol{f}_k$ lies in the null space of $\widetilde{\boldsymbol{H}}_k$, i.e.,

$$\widetilde{\boldsymbol{H}}_k \boldsymbol{f}_k = 0 \ , \ \forall k \in \mathcal{K}, \tag{7}$$

which requires

$$M_t > K - 1. \tag{8}$$

For

$$\boldsymbol{G}_k \triangleq \left[\boldsymbol{G}_k^0;\ \boldsymbol{G}_k^1;\ \cdots;\ \boldsymbol{G}_k^S\right] \in \mathbb{C}^{M_t\times d} \tag{9}$$

where $\boldsymbol{G}_k^s \in \mathbb{C}^{M_s\times d}$ consists of orthonormal columns, which are the base in the null space of $\widetilde{\boldsymbol{H}}_k$, it is true that

$$\boldsymbol{f}_k = \boldsymbol{G}_k \boldsymbol{t}_k, \tag{10}$$

with $\boldsymbol{t}_k \in \mathbb{C}^d$, i.e.

$$\boldsymbol{f}_k^s = \boldsymbol{G}_k^s \boldsymbol{t}_k, s \in \mathcal{S}, k \in \mathcal{K}. \tag{11}$$

Here

$$d \triangleq M_t - K + 1, \tag{12}$$

represents the degree of freedom in designing beamformer vector $\mathbf{f}_k$.

The information throughput (5) at user k is then represented in terms of $\boldsymbol{t}_k$ as

$$C_k(\boldsymbol{t}_k) = \ln(1 + |\overline{\boldsymbol{h}}_k \boldsymbol{t}_k|^2/\sigma_k^2) \tag{13}$$

where $\overline{\boldsymbol{h}}_k \triangleq \boldsymbol{h}_k \boldsymbol{G}_k$.

The total power consumption (6) is expressed in terms of $\mathbf{T} = (\boldsymbol{t}_1, \cdots, \boldsymbol{t}_K)$ as

$$P^{\mathsf{total}}(\mathbf{T}) = \sum_{s=0}^{S} \frac{1}{\lambda_s} \sum_{k=1}^{K} ||\boldsymbol{G}_k^s \boldsymbol{t}_k||^2 + P^{\mathsf{cir}}. \tag{14}$$

We aim at solving the following EE maximization problem (EEM)

$$\max_{\mathbf{T}} \quad \frac{\sum_{k=1}^K \ln(1 + |\overline{\boldsymbol{h}}_k \boldsymbol{t}_k|^2/\sigma_k^2)}{\sum_{s=0}^S \frac{1}{\lambda_s} \sum_{k=1}^K ||\boldsymbol{G}_k^s \boldsymbol{t}_k||^2 + P^{\mathsf{cir}}} \quad \text{s.t.} \tag{15a}$$

$$\ln(1 + |\overline{\boldsymbol{h}}_k \boldsymbol{t}_k|^2/\sigma_k^2) \geq \overline{C}_k, \ k \in \mathcal{K}, \tag{15b}$$

$$\sum_{k\in\mathcal{K}} ||\boldsymbol{G}_k^s \boldsymbol{t}_k||^2 \leq P_{\max}^s, \ s \in \mathcal{S}, \tag{15c}$$

$$\sum_{k=1}^{K} \left[\boldsymbol{G}_k^s \boldsymbol{t}_k (\boldsymbol{G}_k^s \boldsymbol{t}_k)^H\right]_{\ell,\ell} \leq P_{\ell,\max}^s, \tag{15d}$$

$$\ell = 1, ..., M_s \ , \ s \in \mathcal{S},$$

where the EE objective in (15a) is the ratio between the total network throughput and the total transmission power. The constraint in (15b) imposes a QoS throughput requirement on each user k, namely its throughput must be larger than or equal to a predetermined threshold $\overline{C}_k$. Constraints (15c) and (15d) are the sum power and per-antenna power constraints at BS s, respectively.

Note that the numerator in the objective function in (15a) is not a concave function. Therefore the objective function in (15a) is not a ratio of a concave function and a convex function. Also, (15b) is nonconvex constraints. In other words, each Dinkelbach type's iteration, which aims at solving

$$\max_{\mathbf{T}} \quad \sum_{k=1}^{K} \ln(1 + |\overline{\boldsymbol{h}}_k \boldsymbol{t}_k|^2/\sigma_k^2)$$

$$-\tau(\sum_{s=0}^{S} \frac{1}{\lambda_s} \sum_{k=1}^{K} ||\boldsymbol{G}_k^s \boldsymbol{t}_k||^2 + P^{\mathsf{cir}}) \tag{16a}$$

$$\text{s.t.} \quad (15b) - (15d) \tag{16b}$$

in finding τ such that the optimal value of (16) is zero,[1] is computationally intractable because (16) is still a nonconvex program. SDR was used to addressed (16) in [19], however, this method may yield poor performance and inconsistency in this instance [20].

Our next section will provide a path-following computational procedure to address EEM (15) directly bypassing the computationally prohibitive optimization problem (16).

III. Proposed Method

Firstly, as observed in [23], for $\bar{\boldsymbol{t}}_k \triangleq e^{-\jmath.\arg(\overline{\boldsymbol{h}}_k \boldsymbol{t}_k)} \boldsymbol{t}_k$, one has $|\overline{\boldsymbol{h}}_k \boldsymbol{t}_k| = \overline{\boldsymbol{h}}_k \bar{\boldsymbol{t}}_k = \Re\{\overline{\boldsymbol{h}}_k \bar{\boldsymbol{t}}_k\} \geq 0$ in (15a) and (15b) while $||\boldsymbol{G}_k^s \boldsymbol{t}_k||^2 = ||\boldsymbol{G}_k^s \bar{\boldsymbol{t}}_k||^2$ and $\boldsymbol{G}_k^s \boldsymbol{t}_k (\boldsymbol{G}_k^s \boldsymbol{t}_k)^H = \boldsymbol{G}_k^s \bar{\boldsymbol{t}}_k (\boldsymbol{G}_k^s \bar{\boldsymbol{t}}_k)^H$ for all $(k, s) \in \mathcal{K} \times \mathcal{S}$ in (15c) and (15d). Therefore, $|\overline{\boldsymbol{h}}_k \boldsymbol{t}_k|^2$ in (15a) and (15b) can be equivalently replaced by

$$(\Re\{\overline{\boldsymbol{h}}_k \boldsymbol{t}_k\})^2$$

with

$$\Re\{\overline{\boldsymbol{h}}_k \boldsymbol{t}_k\} \geq 0, k \in \mathcal{K}. \tag{17}$$

The nonconvex constraint (15b) is equivalent to the convex constraint

$$\Re\{\overline{\boldsymbol{h}}_k \boldsymbol{t}_k\} \geq \sigma_k \sqrt{e^{\overline{C}_k} - 1}, k \in \mathcal{K}. \tag{18}$$

By using an additional scalar variable t satisfying the convex constraint

$$\sum_{s=0}^{S} \frac{1}{\lambda_s} \sum_{k=1}^{K} ||\boldsymbol{G}_k^s \boldsymbol{t}_k||^2 + P^{\mathsf{cir}} \leq t, \tag{19}$$

[1] such τ obviously is the optimal value of (15)

This article has been accepted for publication in a future issue of this journal, but has not been fully edited. Content may change prior to final publication. Citation information: DOI 10.1109/ACCESS.2016.2626363, IEEE Access

EEM (15) is equivalently expressed by

$$\max_{\mathbf{T},t} \quad f(\mathbf{T},t) = \frac{\sum_{k=1}^{K} \ln(1+(\Re\{\overline{\boldsymbol{h}}_k \boldsymbol{t}_k\})^2/\sigma_k^2)}{t} \quad (20a)$$

$$\text{s.t.} \qquad (15c), (15d), (18), (19). \quad (20b)$$

Initialized by a feasible point $\mathbf{T}^{(0)}$ for the convex constraints (20b) and

$$t^{(0)} = \sum_{s\in\mathcal{S}} \frac{1}{\lambda_s} \sum_{k\in\mathcal{K}} ||\boldsymbol{G}_k^s \boldsymbol{t}_k^{(0)}||^2 + P^{\mathsf{cir}}$$

we process the following successive approximations for $\kappa = 0, 1, \ldots$:

Step 1. Using the inequality

$$x^2 \geq 2x\bar{x} - \bar{x}^2 \quad \forall\ x>0, \bar{x}>0 \quad (21)$$

to obtain

$$(\Re\{\overline{\boldsymbol{h}}_k \boldsymbol{t}_k\})^2 \geq 2\Re\{\overline{\boldsymbol{h}}_k \boldsymbol{t}_k\}\Re\{\overline{\boldsymbol{h}}_k \boldsymbol{t}_k^{(\kappa)}\} - (\Re\{\overline{\boldsymbol{h}}_k \boldsymbol{t}_k^{(\kappa)}\})^2, \quad (22)$$

over the trust region

$$2\Re\{\overline{\boldsymbol{h}}_k \boldsymbol{t}_k\} \geq \Re\{\overline{\boldsymbol{h}}_k \boldsymbol{t}_k^{(\kappa)}\}, k \in \mathcal{K}. \quad (23)$$

Step 2. Using the inequality

$$\ln(1+z) \geq \ln(1+\bar{z}) + \frac{\bar{z}}{\bar{z}+1} - \frac{\bar{z}^2}{\bar{z}+1}\frac{1}{z} \quad \forall\ z>0, \bar{z}>0, \quad (24)$$

whose proof is given in the Appendix, to obtain

$$\begin{aligned} \ln(1+(\Re\{\overline{\boldsymbol{h}}_k \boldsymbol{t}_k\})^2/\sigma_k^2) &\geq \\ \ln(1+(2\Re\{\overline{\boldsymbol{h}}_k \boldsymbol{t}_k\}\Re\{\overline{\boldsymbol{h}}_k \boldsymbol{t}_k^{(\kappa)}\} & \\ -(\Re\{\overline{\boldsymbol{h}}_k \boldsymbol{t}_k^{(\kappa)}\})^2)/\sigma_k^2) &\geq \\ a_k^{(\kappa)} - \frac{b_k^{(\kappa)}}{2c_k^{(\kappa)}\Re\{\overline{\boldsymbol{h}}_k \boldsymbol{t}_k\} - d_k^{(\kappa)}} & \end{aligned} \quad (25)$$

for

$$c_k^{(\kappa)} \triangleq \Re\{\overline{\boldsymbol{h}}_k \boldsymbol{t}_k^{(\kappa)}\} > 0, \quad (26a)$$

$$d_k^{(\kappa)} \triangleq (\Re\{\overline{\boldsymbol{h}}_k \boldsymbol{t}_k^{(\kappa)}\})^2 > 0, \quad (26b)$$

$$a_k^{(\kappa)} \triangleq \ln(1+d_k^{(\kappa)}/\sigma_k^2) + \frac{d_k^{(\kappa)}}{\sigma_k^2 + d_k^{(\kappa)}} > 0, \quad (26c)$$

$$b_k^{(\kappa)} \triangleq (d_k^{(\kappa)})^2/(\sigma_k^2 + d_k^{(\kappa)}) > 0. \quad (26d)$$

Step 3. Using the inequality

$$1/t \geq 2/\bar{t} - t/\bar{t}^2 \quad \forall\ t>0, \bar{t}>0 \quad (27)$$

to obtain

$$\frac{\sum_{k=0}^{K} \ln(1+(\Re\{\overline{\boldsymbol{h}}_k \boldsymbol{t}_k\})^2/\sigma_k^2)}{t} \geq f^{(\kappa)}(\boldsymbol{T},t) \quad (28)$$

for the concave function

$$\begin{aligned} f^{(\kappa)}(\boldsymbol{T},t) \quad \triangleq \quad & a^{(\kappa)}\left(\frac{2}{t^{(\kappa)}} - \frac{t}{(t^{(\kappa)})^2}\right) \\ & - \sum_{k=1}^{K} \frac{b_k^{(\kappa)}}{t(2c_k^{(\kappa)}\Re\{\overline{\boldsymbol{h}}_k \boldsymbol{t}_k\} - d_k^{(\kappa)})}, \end{aligned} \quad (29)$$

where

$$0 < a^{(\kappa)} \triangleq \sum_{k=1}^{K} a_k^{(\kappa)}. \quad (30)$$

Step 4. Solve the convex quadratic program (QP)

$$\max_{\mathbf{T},t} \ f^{(\kappa)}(\boldsymbol{T},t) \quad \text{s.t.} \quad (20b), (23), \quad (31)$$

which is an inner convex approximation [24] of the nonconvex program (20), to generate the next feaxible point $(\mathbf{T}^{(\kappa+1)}, t^{(\kappa+1)})$.

Using (31), in Algorithm 1, we propose a QP-based path-following algorithm to solve EEM (20). The initial point $(\mathbf{T}^{(0)}, t^{(0)})$ for (20) is easily located because all the constraints in (20) are convex.

Algorithm 1 : Path-following algorithm for the EEM (20)

1: **Initialization**: Choose a feasible point $(\mathbf{T}^{(0)}, t^{(0)})$ for (20). Set $\kappa := 0$.
2: **Repeat**
3: Solve the QP (31) for the optimal solution $(\mathbf{T}^{(\kappa+1)}, t^{(\kappa+1)})$.
4: Set $\kappa := \kappa + 1$.
5: **Until** convergence of the objective in (20).

Proposition 1: Algorithm 1 generates a sequence $\{(\mathbf{T}^{(\kappa)}, t^{(\kappa)})\}$ of improved points for (20), which converges to a Karush-Kuhn-Tucker (KKT) point.

Proof. Note that

$$f(\mathbf{T},t) \geq f^{(\kappa)}(\mathbf{T},t)\ \forall\ \mathbf{T},t$$

and

$$f(\mathbf{T}^{(\kappa)}, t^{(\kappa)}) = f^{(\kappa)}(\mathbf{T}^{(\kappa)}, t^{(\kappa)}).$$

Hence, as far as $(\mathbf{T}^{(\kappa+1)}, t^{(\kappa+1)}) \neq (\mathbf{T}^{(\kappa)}, t^{(\kappa)})$:

$$\begin{aligned} f(\mathbf{T}^{(\kappa+1)}, t^{(\kappa+1)}) &\geq f^{(\kappa)}(\mathbf{T}^{(\kappa+1)}, t^{(\kappa+1)}) \\ &> f^{(\kappa)}(\mathbf{T}^{(\kappa)}, t^{(\kappa)}) \\ &= f(\mathbf{T}^{(\kappa)}, t^{(\kappa)}), \end{aligned}$$

where the second inequality follows from the fact that $(\mathbf{T}^{(\kappa+1)}, t^{(\kappa+1)})$ and $(\mathbf{T}^{(\kappa)}, t^{(\kappa)})$ are the optimal solution and a feasible point of (31), respectively. This result shows that $(\mathbf{T}^{(\kappa+1)}, t^{(\kappa+1)})$ is a better point to (20) than $(\mathbf{T}^{(\kappa)}, t^{(\kappa)})$.

This article has been accepted for publication in a future issue of this journal, but has not been fully edited. Content may change prior to final publication. Citation information: DOI 10.1109/ACCESS.2016.2626363, IEEE Access

Furthermore, the sequence $\{(\mathbf{T}^{(\kappa)}, t^{(\kappa)})\}$ is bounded by constraints in (20b). By Cauchy's theorem, there is a convergent subsequence $\{(\mathbf{T}^{(\kappa_\nu)}, t^{(\kappa_\nu)})\}$ with a limit point $(\bar{\mathbf{T}}, \bar{t})$, i.e.,

$$\lim_{\nu \to +\infty} \Big[f(\mathbf{T}^{(\kappa_\nu)}, t^{(\kappa_\nu)}) - f(\bar{\mathbf{T}}, \bar{t}) \Big] = 0.$$

For every κ, there is ν such that $\kappa_\nu \leq \kappa \leq \kappa_{\nu+1}$, so

$$\begin{aligned} 0 &= \lim_{\nu \to +\infty} [f(\mathbf{T}^{(\kappa_\nu)}, t^{(\kappa_\nu)}) - f(\bar{\mathbf{T}}, \bar{t})] \\ &\leq \lim_{\kappa \to +\infty} [f(\mathbf{T}^{(\kappa)}, t^{(\kappa)}) - f(\bar{\mathbf{T}}, \bar{t})] \\ &\leq \lim_{\nu \to +\infty} [f(\mathbf{T}^{(\kappa_{\nu+1})}, t^{(\kappa_{\nu+1})}) - f(\bar{\mathbf{T}}, \bar{t})] \\ &= 0, \end{aligned}$$

which shows that

$$\lim_{\kappa \to +\infty} f(\mathbf{T}^{(\kappa)}, t^{(\kappa)}) = f(\bar{\mathbf{T}}, \bar{t}).$$

Each accumulation point $\{(\bar{\mathbf{T}}, \bar{t})\}$ of the sequence $\{(\mathbf{T}^{(\kappa)}, t^{(\kappa)})\}$ is indeed a KKT point according to [25, Th. 1].

IV. Sparse beamforming for the three-objective optimization

For realizing the outcome of the EE maximization problem (15), it requires that the CP must upload all $\mathbf{f}_k^s x_k$ to all SBSs. Intuitively, due to its low power and short range of coverage, each SBS is unable to contribute much in conveying symbols intended for those users, who are out of its effective coverage range. Therefore, it may be not efficient to offload the symbols intended for these users to it. In this section, we consider EEM (15) in the context of sparse

$$\mathbf{F} = [\mathbf{f}_k^s]_{(k,s) \in \mathcal{K} \times (\mathcal{S} \setminus \{0\})}, \tag{32}$$

as $\mathbf{f}_k^s \approx 0$ means that there is no need to offload $\mathbf{f}_k^s x_k$ for user k to SBS s.

This motivates us to consider the following optimization to promote its sparsity [26]

$$\begin{aligned} \max_{\mathbf{T}, t} \quad & f(\mathbf{T}, t) - \gamma \sum_{(k,s) \in \mathcal{K} \times (\mathcal{S} \setminus \{0\})} \ln(1 + ||\mathbf{G}_k^s \mathbf{t}_k||^2 / \epsilon) \\ \text{s.t.} \quad & (20b), \end{aligned} \tag{33}$$

where $0 < \epsilon << 1$ and $\gamma > 0$ is the sparsity penalty parameter. In what follows we call (33) three-objective optimization problem (3OO) because by considering (33) we incorporate simultaneous three objectives: EE, users's QoS and BS association for serving the users.

It is obvious that the inclusion of the nonconvex function $\gamma \sum_{(k,s) \in \mathcal{K} \times (\mathcal{S} \setminus \{0\})} \ln(1 + ||\mathbf{G}_k^s \mathbf{t}_k||^2 / \epsilon)$ in the objective in (33) makes the latter more computationally challenging than EEM (15). However, we will see shortly that a QP-based path-following computational procedure is still available for addressing 3OO (33).

Using the inequality

$$\ln(1 + x) \leq \ln(1 + \bar{x}) + \frac{x - \bar{x}}{1 + \bar{x}} \quad \forall\ x \geq 0, \bar{x} \geq 0,$$

which follows from the concavity of function $\ln(1 + x)$, for $(\mathbf{T}^{(\kappa)}, t^{(\kappa)})$ which is feasible for (20b), the following inequality holds true

$$\ln(1 + ||\mathbf{G}_k^s \mathbf{t}_k||^2 / \epsilon) \ \leq \ g_{k,s}^{(\kappa)}(\mathbf{t}_k), \tag{34}$$

with

$$\begin{aligned} g_{k,s}^{(\kappa)}(\mathbf{t}_k) \ \triangleq \ & \ln(1 + ||\mathbf{G}_k^s \mathbf{t}_k^{(\kappa)}||^2 / \epsilon) \\ & + \frac{||\mathbf{G}_k^s \mathbf{t}_k||^2 - ||\mathbf{G}_k^s \mathbf{t}_k^{(\kappa)}||^2}{\epsilon + ||\mathbf{G}_k^s \mathbf{t}_k^{(\kappa)}||^2}. \end{aligned} \tag{35}$$

Recalling that $f^{(\kappa)}(\boldsymbol{T}, t)$ defined from (29) is a lower bound of $f(\boldsymbol{T}, t)$, the following QP

$$\begin{aligned} \max_{\mathbf{T}, t} \quad & f^{(\kappa)}(\boldsymbol{T}, t) - \sum_{(k,s) \in \mathcal{K} \times (\mathcal{S} \setminus \{0\})} g_{k,s}^{(\kappa)}(\mathbf{t}_k) \\ \text{s.t.} \quad & (20b), (19), (23), \end{aligned} \tag{36}$$

which is solved at κth iteration to generate the next feasible point $(\mathbf{T}^{(\kappa+1)}, t^{(\kappa+1)})$, is an inner approximation of 3OO (33).

Using (36), in Algorithm 2, we propose a QP-based path-following algorithm to solve 3OO (33). Its convergence is proved similarly to Proposition 1.

Algorithm 2 : Path-following algorithm for 3OO (33)

1: **Initialization**: Choose a feasible point $(\mathbf{T}^{(0)}, t^{(0)})$ for (20). Set $\kappa := 0$.
2: **Repeat**
3: Solve the QP (36) for the optimal solution $(\mathbf{T}^{(\kappa+1)}, t^{(\kappa+1)})$.
4: Set $\kappa := \kappa + 1$.
5: **Until** convergence of the objective in (33).

V. Numerical Results and Discussions

In this section, we use numerical examples to evaluate the performance of the proposed algorithms. The MBS is equipped with $M_0 = 10$ antennas and is located at the marco cell centre. All $S = 4$ SBSs are equipped with $M_s \equiv 2$ antennas, which are uniformly distributed in the macro cell. $K = 14$ users are randomly distributed but there is at least one user in the coverage area of each SBS as shown in Fig. 2. The channel model is generated by the simulation parameters are provided in Table I, which mainly follow those studied in prior works [10], [27]. We

This article has been accepted for publication in a future issue of this journal, but has not been fully edited. Content may change prior to final publication. Citation information: DOI 10.1109/ACCESS.2016.2626363, IEEE Access

also set $\overline{C}_k \equiv 0.2$ bps/Hz for QoS constraint (15b) and $P_s^{\max} \equiv P_{sbs}$ for $s \geq 1$ and $P_{\ell,\max}^s = P_s^{\max}/M_s$ for per-antenna power constraints (15d). We set $\epsilon = 10^{-6}$ and $\gamma = 10^{-5}$ in solving 3OO (33).

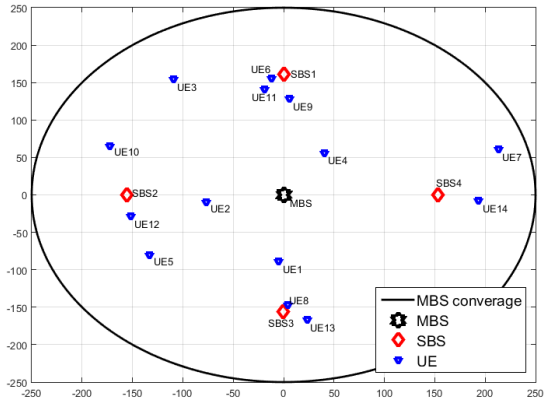

Fig. 2. The scenario of HetNet.

TABLE I
SIMULATION SETUP

Parameter	Assumption
Macro-cell coverage	250m
Small-cell coverage	50m
Distance between MBS and SBSs	$\geq$ 150m
Distance between MBS and users	$\geq$ 50m
Carrier frequency / Bandwidth	2 Gz / 10 MHz
Maximal MBS power	$P_{\max}^0 = P_0$ = 43 dBm
Maximal SBS power	$P_{\max}^s = P_{sbs}$ = 30 dBm
Path loss from MBS to user	128.1+37.6log$_{10}$ R [dB], R in km
Path loss from SBS to user	140.7+36.7log$_{10}$ R [dB], R in km
Shadowing standard deviation	8dB
Noise power density	-174 dBm/Hz
The power amplifiers parameter	$\lambda_0 = 0.388$, $\lambda_s = 0.052$
The circuit power per antenna	P_m = 189 mW, , P_n = 5.6 mW
The non-transmission power	$P_{c,0}$ = 40 dBm , $P_{c,s}$ = 20 dBm

Fig. 3 demonstrates a typical convergence of Algorithm 1 and Algorithm 2 for a representative channel realization. Algorithm 1 and Algorithm 2 converge within 10 iterations. Interestingly, the EE part in the objective in (33) also iteratively increases.

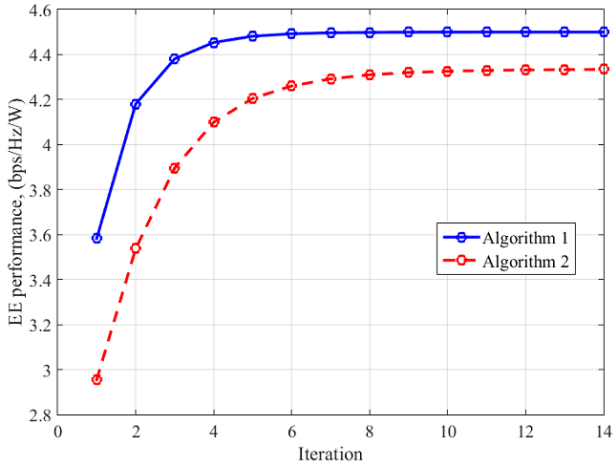

Fig. 3. The convergence of Algorithm 1 for EE performance.

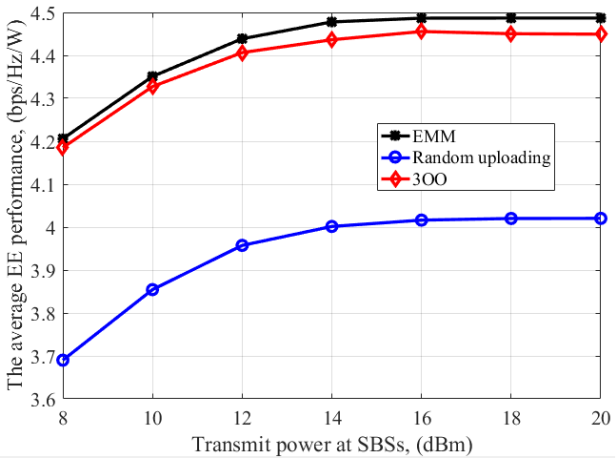

Fig. 4. The average EE performance versus the allowed transmit power P_s at SBSs.

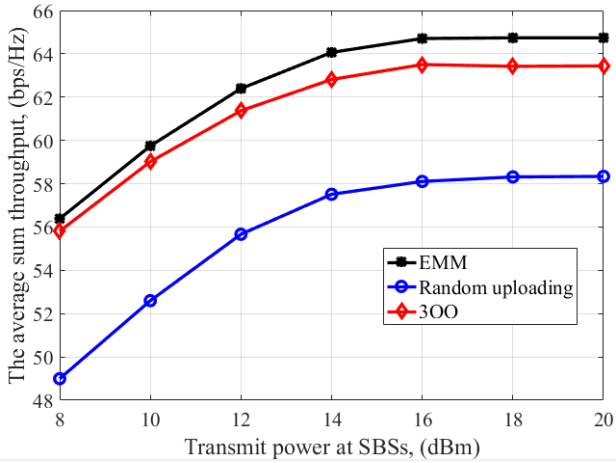

Fig. 5. The average sum throughput versus the allowed transmit power P_s at SBSs.

We observe an obvious gap in EE performance and corresponding sum throughput between EEM (20) and

This article has been accepted for publication in a future issue of this journal, but has not been fully edited. Content may change prior to final publication. Citation information: DOI 10.1109/ACCESS.2016.2626363, IEEE Access

SBS	UE1	UE2	UE3	UE4	UE5	UE6	UE7	UE8	UE9	UE10	UE11	UE12	UE13	UE14
SBS 1	**Off**	On	**Off**	**Off**	On	On	**Off**	**Off**	On	On	On	**Off**	**Off**	**Off**
SBS 2	**Off**	**Off**	**Off**	**Off**	**Off**	**Off**	**Off**	**Off**	**Off**	**Off**	**Off**	On	**Off**	**Off**
SBS 3	On	On	**Off**	On	On	**Off**	**Off**	On	**Off**	**Off**	**Off**	**Off**	On	**Off**
SBS 4	**Off**	**Off**	**Off**	**Off**	**Off**	**Off**	On	**Off**	**Off**	**Off**	**Off**	**Off**	**Off**	On

TABLE II
SBS ASSOCIATION IN 3OO.

3OO (33) in Fig. 4 and Fig. 5. Table II shows users' association of each SBS for service under a representative channel realization. The CP has to upload only 13 intended beamformed symbols to SBSs in 3OO (33) instead of uploading all 56 beamformed symbols in EEM (20). In consistence with Fig. 2, Table II reveals that SBS 4 serves only user 7 and user 14, who are sufficiently close for its effective service. Both users 7 and user 14 are also far away from other SBS so they are served by SBS 4 and MBS only. Indeed, Fig. 2 and Table II confirm that each SBS serve the users, who are closer to it.

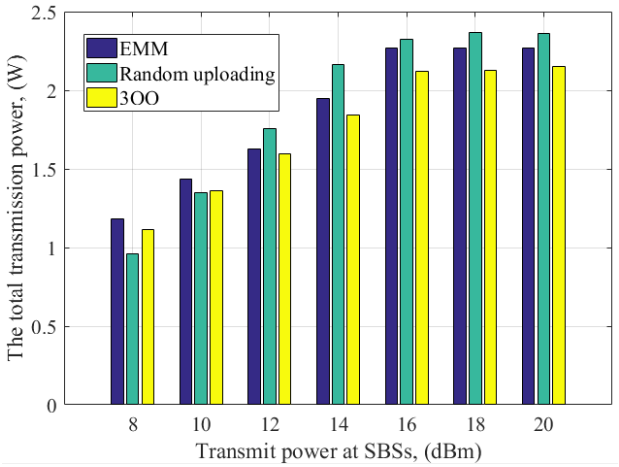

Fig. 6. The average EE performance versus the transmit power constraint P_{sbs}.

To see how the SBS beamformer power in the denominator and the sum throughput in the numerator interplay in optimizing the EE objective in (20) and (33) we vary P_{sbs} in the next simulation. Fig. 4 shows that EE performances saturate when the maximal transmit power P_{sbs} at SBSs passes a specific threshold 16 dBm. When the beamformer power is constrained small, the denominator of the EE objective in (20) and (33) defined from (6) is dominated by the constant circuit power P^{cir} so the EE objective is maximized by maximizing its numerator. In contrast, the EE objective is likely maximized by minimizing its denominator once the latter is dominated by the beamformer power. This explains that both EE objective and its numerator saturate in Fig. 4 and Fig. 5 for P_{sbs} beyond the value 16 dBm in the simulation. Interestingly, Fig. 6 also supports this observation: the actual transmit power is increased to improve the sum throughput for P_{sbs} from 8 dBm to 16 dBm and then saturates for $P_{sbs} > 16$ dBm, where it is kept minimal. This means the value $P_s = 16$ dBm is the best power constraint for the network EE. We also observe that 3OO (33) utilizes less power than EEM (20) in optimizing EE.

To show the efficiency of 3OO (33) we also include in Fig. 4-6 the EE performance and the corresponding sum throughput and transmit power when the CP randomly uploads $\mathbf{f}_k^s x_k$ to SBS s as follows. For each SBS s, take randomly three user k for setting the additional constraints $||\mathbf{G}_k^s \mathbf{t}_k||^2 \leq 10^{-4}$ in solving EEM (20).

Next, we investigate the impact of the QoS thresholds $\overline{C}_k$ in (15b) to the EE performance in EEM (20) and 3OO (33). Under the SBS beamformer power limit in Table I, the EE performance does not seem to be sensitive to varied $\overline{C}_k \equiv \bar{C}$. For simulating Fig. 7 we set $\overline{C}_k \equiv \bar{C}$ only for those users, who are not in a coverage range of any SBS. For other users we set the threshold $3\bar{C}$. According to Fig. 7 the EE performance in the three methods does not drop much until $\bar{C}$ becomes larger than a specific value of 1.6 bps/Hz. This specific value of $\bar{C}$ is optimal for balancing the three mentioned optimization objectives. Fig. 8 also supports this point: with $\bar{C}$ larger than 1.6 bps/Hz, a substantial increase in the SBS transmit beamforming power is needed to meet such high QoS. As a result, the denominator increases substantially in the EE objective in (20) and (33) but the numerator remains almost flat as Fig. 9 shows. Consequently, the corresponding EE objective is dropped.

This article has been accepted for publication in a future issue of this journal, but has not been fully edited. Content may change prior to final publication. Citation information: DOI 10.1109/ACCESS.2016.2626363, IEEE Access

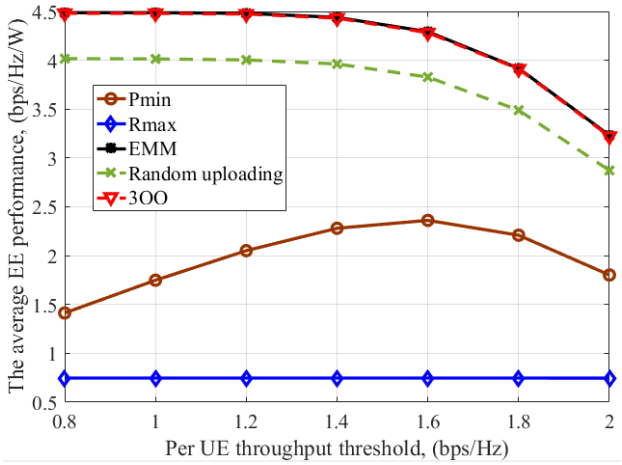

Fig. 7. The average EE performance versus per-user throughput threshold.

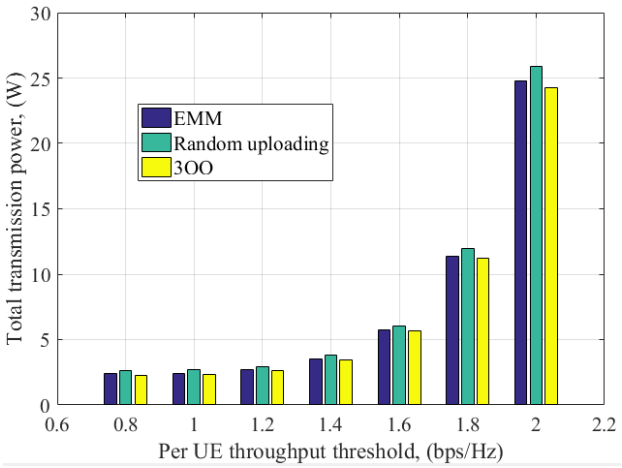

Fig. 8. The average throughput versus per-user throughput threshold.

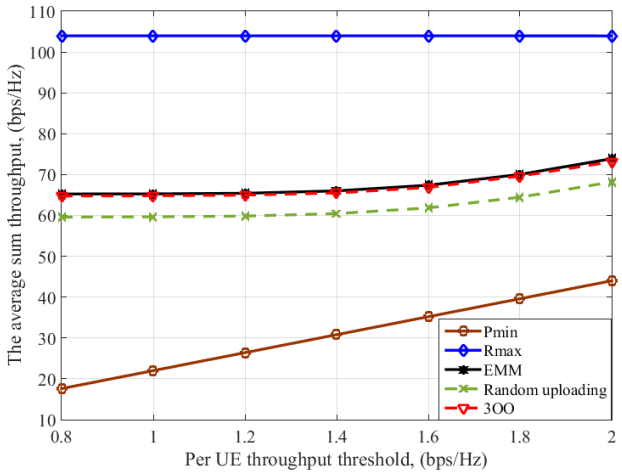

Fig. 9. The average sum throughput versus per-user throughput threshold.

We also compare the EE performance with that by minimizing the dominator and maximizing the numerator of the EE objective in (20) [13], [14]:

$$\text{Pmin:} \quad \min_{\mathbf{T}} \ \sum_{s=0}^{S}\sum_{k=1}^{K} ||\boldsymbol{G}_k^s \boldsymbol{t}_k||^2 \quad \text{s.t.} \quad (15b), (15c), (15d) \tag{37}$$

and

$$\text{Rmax:} \quad \max_{\mathbf{T}} \ \sum_{k=1}^{K} \ln(1+|\bar{\boldsymbol{h}}_k \boldsymbol{t}_k|^2/\sigma_k^2) \quad \text{s.t.} \quad (15b), (15c), (15d). \tag{38}$$

Interestingly, according to Fig. 7, $\bar{C} = 1.6$ bps/Hz is also optimal for balancing three objectives in the beamformer power optimization problem (37). Additionally, using the sum throughput maximization problem (38) is not recommended for addressing the network EE.

VI. Conclusions

We have presented a cooperative beamforming design for maximizing the EE of a two-tier HetNet, where three-objective (EE, QoS, service loading) were incorporated. As the commonly used Dinkelbach type algorithms are no longer applicable to our problems, we have developed path-following algorithms for computational solution, which quickly converge at least to a locally optimal solution. The numerical results have been provided to demonstrate the usefulness and merit of the developed algorithms.

Appendix: Proof for (24)

Note that function $\eta(x) = \ln(1+1/x)$ is convex in $x > 0$. Therefore, for any $x > 0$ and $\bar{x} > 0$, it is true that [24]

$$\begin{aligned} \ln(1+1/x) &\geq \ln(1+1/\bar{x}) + \frac{\partial \eta(\bar{x})}{\partial x}(x-\bar{x}) \\ &= \ln(1+\frac{1}{\bar{x}}) + \frac{1}{1+\bar{x}} \\ &\quad -\frac{1}{(1+\bar{x})\bar{x}}x. \end{aligned} \tag{39}$$

Then (24) is obtained by replacing $z = 1/x$ and $\bar{z} = 1/\bar{x}$ into (39).

References

[1] J. Andrews, "Seven ways that HetNets are a cellular paradigm shift," *IEEE Commun. Mag.*, vol. 51, no. 3, pp. 136–144, Mar. 2013.

[2] E. Hossain, M. Rasti, H. Tabassum, and A. Abdelnasser, "Evolution toward 5G multi-tier cellular wireless networks: An interference management perspective," *IEEE Wireless Commun. Mag.*, vol. 21, no. 3, pp. 118–127, Jun. 2014.

[3] Q. Li, H. Niu, A. Papathanassiou, and G. Wu, "5G network capacity: Key elements and technologies," *IEEE Veh. Technol. Mag.*, vol. 9, no. 1, pp. 71–78, March 2014.

[4] V. Chandrasekhar, M. Kountouris, and J. G. Andrews, "Coverage in multi-antenna two-tier networks," *IEEE Trans. Wireless Commun.*, vol. 8, no. 10, pp. 5314–5327, 2009.

[5] M. Rihan, M. Elsabrouty, O. Muta, and H. Fumkawa, "Iterative interference alignment in macrocell-femtocell networks: A cognitive radio approach," in *Proc. Int. Symp. on Wireless Commun. System (ISWCS)*, Aug 2014, pp. 654–658.

[6] A. Fehske, G. Fettweis, J. Malmodin, and G. Biczok, "The global footprint of mobile communications: The ecological and economic perspective," *IEEE Commun. Magazine*, vol. 49, no. 8, pp. 55–62, 2011.

[7] R. L. G. Cavalcante, S. Stanczak, M. Schubert, A. Eisenlatter, and U. Turke, "Toward energy-efficienct 5G wireless communications technologies," *IEEE Signal Process. Magazine*, vol. 13, no. 11, pp. 24–34, Nov. 2014.

[8] C. I, C. Rowelll, S. Han, Z. Xu, G. Li, and Z. Pan, "Toward green and soft: a 5G perspective," *IEEE Commun. Magazine*, vol. 13, no. 2, pp. 66–73, Feb. 2014.

[9] Y. S. Soh, T. Q. Quek, M. Kountouris, and H. Shin, "Energy efficient heterogeneous cellular networks," *IEEE J. Sel. Areas Commun.*, vol. 31, no. 5, pp. 840–850, May 2013.

[10] E. Bjornson, M. Kountouris, and M. Debbah, "Massive MIMO and small cells: Improving energy efficiency by optimal soft-cell coordination," in *Proc. IEEE ICT*, May 2013, pp. 1–5.

[11] J. Li, E. Bjornson, T. Svensson, T. Eriksson, and M. Debbah, "Joint precoding and load balancing optimization for energy-efficient heterogeneous networks," *IEEE Trans. Wireless Commun.*, vol. 14, no. 10, pp. 5810–5822, 2015.

[12] E. Bjornson, L. Sanguinetti, and M. Kountouris, "Deploying dense networks for maximal energy efficiency: Small cells meet massive MIMO," *IEEE J. on Selected Areas in Commun.*, vol. 34, no. 4, pp. 832–847, 2016.

[13] Z. Xu, C. Yang, G. Y. Li, Y. Liu, and S. Xu, "Energy-efficient CoMP precoding in heterogeneous networks," *IEEE Trans. Signal Process.*, vol. 62, no. 4, pp. 1005–1017, Feb 2014.

[14] W.-C. Liao, M. Hong, Y.-F. Liu, and Z.-Q. Luo, "Base station activation and linear transceiver design for optimal resource management in heterogeneous networks," *IEEE Trans. Signal Process.*, vol. 62, no. 15, pp. 3939–3952, Aug 2014.

[15] L. D. Nguyen, T. Q. Duong, D. N. Nguyen, and L.-N. Tran, "Energy efficiency maximization for heterogeneous networks: A joint linear precoder design and small-cell switching-off approach," in *Proc. IEEE GlobalSIP 2016*, Dec 2016, to appear.

[16] W. Dinkelbach, "On nonlinear fractional programming," *Management Science*, vol. 13, no. 7, pp. 492–498, 1967.

[17] S. He, Y. Huang, S. Jin, and L. Yang, "Coordinated beamforming for energy efficient transmission in multicell multiuser systems," *IEEE Trans. Commun.*, vol. 61, no. 12, pp. 4961–4971, 2013.

[18] O. Tervo, L.-N. Tran, and M. Juntti, "Optimal energy-efficient transmit beamforming for multi-user MISO downlink," *IEEE Trans. Signal Process.*, vol. 63, no. 20, pp. 5574–5588, 2015.

[19] Q.-D. Vu, L.-N. Tran, R. Farrell, and E.-K. Hong, "Energy-efficient zero-forcing precoding design for small-cell networks," *IEEE Trans. Commun.*, vol. 64, no. 2, pp. 790–804, Feb 2016.

[20] A. H. Phan, H. D. Tuan, H. H. Kha, and D. T. Ngo, "Nonsmooth optimization for efficient beamforming in cognitive radio multicast transmission," *IEEE Trans. Signal Process.*, vol. 60, no. 6, pp. 2941–2951, 2012.

[21] Z. Shen, R. Chen, J. G. Andrews, R. W. Heath, and B. L. Evans, "Sum capacity of multiuser MIMO broadcast channels with block diagonalization," *IEEE Trans. Wireless Commun.*, vol. 6, no. 6, pp. 2040–2045, 2007.

[22] C. Li, J. Zhang, and K. B. Letaief, "Throughput and energy efficiency analysis of small cell networks with multi-antenna base stations," *IEEE Trans. Wireless Commun.*, vol. 13, no. 5, pp. 2505–2517, May 2014.

[23] A. Wiesel, Y. Eldar, and S. Shamai, "Linear precoding via conic optimization for fixed MIMO receivers," *IEEE Trans. Signal Processing*, vol. 54, no. 1, pp. 161–176, Jan. 2006.

[24] H. Tuy, *Convex Analysis and Global Optimization*. Kluwer Academic, 1997.

[25] B. R. Marks and G. P. Wright, "A general inner approximation algorithm for nonconvex mathematical programs," *Operation Research*, vol. 26, no. 4, pp. 681–683, 1978.

[26] E. J. Candes, M. B. Wakin, and S. P. Boyd, "Enhancing sparsity by reweighted ℓ_1 minimization," *J. of Fourier Anal. Appl.*, vol. 14, no. 5-6, pp. 877–905, Dec 2008.

[27] J. Tang, D. K. C. So, E. Alsusa, K. A. Hamdi, and A. Shojaeifard, "Resource allocation for energy efficiency optimization in heterogeneous networks," *IEEE J. on Selected Areas in Commun.*, vol. 33, no. 10, pp. 2104–2117, Oct 2015.